Published in final edited form as:
J Cataract Refract Surg. 2014 June ; 40(6): 1041–1047. doi:10.1016/j.jcrs.2014.03.017.

Serial biomechanical comparison of edematous, normal, and collagen crosslinked human donor corneas using optical coherence elastography

Matthew R. Ford, BS, **Abhijit Sinha Roy, PhD**, **Andrew M. Rollins, PhD**, and **William J. Dupps Jr, MD, PhD**
Department of Biomedical Engineering (Ford, Rollins), Case Western Reserve University, the Cleveland Clinic Cole Eye Institute (Ford, Sinha Roy, Dupps), and the Department of Biomedical Engineering (Dupps), Cleveland Clinic Lerner Research Institute, Cleveland, Ohio, USA

Abstract

PURPOSE—To noninvasively evaluate the effects of corneal hydration and collagen crosslinking (CXL) on the mechanical behavior of the cornea.

SETTING—Cleveland Clinic Cole Eye Institute, Cleveland, Ohio, USA.

DESIGN—Experimental study.

METHODS—An optical coherence elastography (OCE) technique was used to measure the displacement behavior of 5 pairs of debrided human donor globes in 3 serial states as follows: edematous, normal thickness, and after riboflavin–ultraviolet-A–mediated CXL. During micromotor-controlled axial displacements with a curved goniolens at physiologic intraocular pressure (IOP), serial optical coherence tomography scans were obtained to allow high-resolution intrastromal speckle tracking and displacement measurements over the central 4.0 mm of the cornea.

RESULTS—With no imposed increase in IOP, the mean lateral to imposed axial displacement ratios were 0.035 μm/μm ± 0.037 (SD) in edematous corneas, 0.021 ± 0.02 μm/μm in normal thickness corneas, and 0.014 ± 0.009 μm/μm in post-CXL corneas. The differences were statistically significant ($P<.05$, analysis of variance) and indicated a 40% increase in lateral stromal resistance with deturgescence and a further 33% mean increase in relative stiffness with CXL.

CONCLUSIONS—Serial perturbations of the corneal hydration state and CXL had significant effects on corneal biomechanical behavior. With an axially applied stress from a nonapplanating contact lens, displacements along the direction of the collagen lamellae were 2 orders of magnitude lower than axial deformations. These experiments show the ability of OCE to quantify clinically relevant mechanical property differences under physiologic conditions.

Financial Disclosures—Proprietary or commercial disclosures are listed after the references.

Corresponding author: William J. Dupps Jr, MD, PhD, 9500 Euclid Ave/i-32, Cleveland 44195, Ohio, USA. bjdupps@sbcglobal.net..

The shape of the cornea and its optical properties are greatly influenced by the biomechanical properties of its constituent tissue. Diseases such as keratoconus, pellucid marginal degeneration, and keratoglobus distort this shape and are hypothesized to involve a primary disorder of biomechanical strength.[1] Although stiffening by corneal collagen crosslinking (CXL) is a promising emerging treatment for ectatic disease,[2] the biomechanical features of ectatic disease and the impact of CXL on target tissues have not been fully characterized, in part because of a paucity of clinical tools for biomechanical characterization.[3–6]

Refractive surgery procedures such as laser in situ keratomileusis (LASIK) and photorefractive keratectomy (PRK) are performed to reduce spectacle or contact lens dependence by altering the corneal shape and refractive power. In such procedures, the biomechanical properties of the cornea are altered and mediate secondary mechanical shape changes of the corneal surface.[7,8] In corneas with undiagnosed disease states, refractive surgery can be followed by a progressive and sometimes unrecoverable corneal shape change.[1,9,10] The combination of an ectatic disease state and refractive surgery may lead to rapid corneal degeneration.[9,11,12] Currently available screening tools to detect this type of predisposition do not offer the capability to spatially resolve the mechanical properties of the cornea. Laser in situ keratomileusis, PRK, and other corneal reshaping procedures do not currently account for patient-specific mechanical properties, and the lack of such information may contribute to less predictable refractive outcomes due to interindividual differences in the corneal biomechanical state. These issues point to a need for an in vivo tool for measuring the mechanical properties of the cornea that can enhance the sensitivity and specificity of screening examinations and provide data for modeling the influence of tissue-specific mechanical properties on the surgical outcome.[1,13–15]

Elastography is a method originally pioneered in the field of ultrasound imaging.[16] It provides mechanical contrast to imaging for tissue discrimination. Application of elastographic techniques to optical coherence tomography (OCT)[16–24] has shown promise in distinguishing diseased states from normal tissue states.[25–31] The application of these techniques to the measurement of corneal biomechanical properties could affect early disease detection, enhance assessment of candidacy for corneal refractive procedures, and enable more patient-specific surgical planning.

Elastography of the cornea requires the implementation of an imaging technique and a perturbation protocol. We previously described a nondestructive technique that used a gonioscopy lens to impart stress perturbation and OCT imaging to measure the displacement response throughout the corneal depth.[32,33] The current study sought to determine the biomechanical effect in terms of lateral resistance to displacement of hydration changes and CXL in human whole-globe corneal tissue.

MATERIALS AND METHODS

Five pairs of human donor globes were obtained from Cleveland Eye Bank and used for the experiments. Each eye was tested within 72 hours postmortem, with the majority being used

within 48 hours. The eyes were obtained in a refrigerated, but not frozen, state and preserved in a chondroitin sul-fate–based corneal storage medium (Optisol-GS, Bausch & Lomb).

The following procedure was performed on each eye globe: Once the eye was obtained, it was removed from refrigerated storage. The principal meridia of the eye were identified by the remnants of the ocular muscles still attached to the globe. The eye was mounted beneath a purpose-designed OCT device sample arm and pressurized using gravity-infused 0.9% saline through a 21-gauge needle inserted into the posterior chamber. The pressure inside the globe was monitored with an inline pressure transducer and calibrated digital monitor. The intraocular pressure (IOP) was set to a target of 15 mm Hg and monitored throughout all stages of the experiments. After mounting and pressurization were complete, the epithelium was removed by manual scraping.

The OCT imaging was performed using a previously described technique.[32] The technique consisted of scanning 4.0 mm × 40 μm with lateral oversampling of approximately 10 times the spot size (20 μm) to ensure accurate capture of the speckle pattern. Imaging was performed at a line rate of 47 000 A-scans/sec with no averaging performed. The system consisted of a purpose-built k-space linear Fourier-domain OCT system with 12 μm axial resolution in air and a spot size of approximately 20 μm in air with a scanning range of 15.0 mm by 15.0 mm laterally. The system was driven by a C++ software suite created for this purpose.

While the donor eye was still in an edematous state, the first set of imaging experiments was performed. A standard clinical gonioscopy lens with a 4.0 mm central aperture (Volk Optical, Inc.) was used to perturb the tissue. The OCT sample arm beam was passed through the central unobstructed view of the gonioscopy lens, as in Figure 1. This enabled imaging a window of approximately 4.0 mm in width. The imaging window was oriented along 1 of the 2 principal meridia chosen at random.

The gonioscopy lens was physically mounted to a computer-controlled translation stage (TLA-28, Zaber Technologies, Inc.), which was used to control the displacement of the gonioscopy lens on the cornea (Figure 1). The gonios-copy lens was displaced in 20 μm increments along the scan direction (axially) through a total range of 220 μm. Images were acquired before and after each displacement increment. Displacement tracking was performed using a method previously described.[32] In this study, the region of interest used was 15 pixels by 15 pixels, or 60 μm axially by 15 μm laterally. As before, basic thresholding was used to prevent erroneous tracking of noise in the image. The imaging sequence was repeated for the second meridia to ensure that data were collected in the nasal–temporal and inferior–superior meridia.

After the first imaging sequence was completed, the eye was inflated to approximately 50 mm Hg and a hyperosmolar dextran 15% solution (MW 500 000, Sigma-Aldrich Co.) was applied to the corneal surface to thin the cornea to approximately normal physiologic levels.[34,35] The eye was allowed to thin to normal physiologic thickness (≤500 μm) over approximately 30 minutes. Central corneal thickness (CCT) was measured with the OCT

scanner. After physiologic thickness was achieved, the imaging sequence performed on the edematous cornea was repeated.

After completion of the thinning and second imaging sequence, the eye was prepared for CXL following a standard clinical protocol as follows: One drop of riboflavin 0.1% (concentration) was applied every 5 minutes with an ultraviolet-A (UVA) source (Pria Vision, Inc.) illuminating the cornea at 3 mW/cm^2 and turned on after the application of the second riboflavin drop. The riboflavin solution did not contain dextran. Seven drops over 35 minutes and continuous UVA exposure for 30 minutes completed the CXL protocol. The imaging sequence was repeated for the third and final time after the CXL procedure was completed.

The data were collected for each set of imaging sequences. Each image was divided into 6 sections across the 4.0 mm of the corneal stroma (Figure 2). While the 2 central sections overlap between meridia, the outer 4 sections do not, resulting in 10 regional data sets; that is, the anterior and posterior of nasal, temporal, superior, inferior, and central. Local lateral displacement information in each section was averaged to produce a single data point per section. These lateral displacement measurements were plotted against the corresponding local measured axial displacement. The absolute slope of the resultant line was fitted using a linear fit. The absolute value of the slope was used to compensate for differences in lateral displacement direction between each section of the image because the mechanical properties are insensitive to image orientation. This slope was then processed with a general linear analysis-of-variance statistical model using Minitab statistical software (version 14, Minitab Inc.) to look for differences between the 3 measured states (edematous, deturgesed, and crosslinked), the 10 regions identified previously, the left eye and right eye, and each eye pair. A post hoc Tukey analysis for pairwise multiple comparisons was performed to detect statistically significant differences between the individual groups.

RESULTS

During all compression experiments, the IOP of donor globes remained within 1 mm Hg of pre-perturbation IOP measured with the in-line pressure transducer. The mean change in CCT between edematous and deturgesed states was 88.2 μm ± 69.6 (SD).

Figure 3 shows color elastograms and plots of regional displacement of a representative donor globe. The upper frame in Figure 3, *A*, shows the lateral corneal tissue motion in a post-deturgescence/pre-CXL cornea across an imaged section during axial compression. Displacements on the order of 5 μm or less were observed in most regions, with the areas of greatest displacement (least relative stiffness) indicated in red and corresponding to posterior stroma. Axial compressions were nearly spatially uniform (*lower frame* in Figure 3, A), confirming that the imposed stress delivered by the goniolens did not produce inhomogeneous axial deformations and complex bending moments as one would observe with an applanating or indenting perturbation.

Table 1 shows the mean values (±SD) of the dataset. Data from 1 donor pair obtained while nearby building construction was in progress were eliminated because of potential vibration

artifact and classification as an outlier by the statistical software, with differences in displacement more than double those of all other pairs. There were no statistically significant differences between left and right donor eyes, the 10 corneal regions, or the 2 meridia measured under any tissue state in the eyes as a group. Statistically significant interregional differences were noted in individual eyes; however, interregional differences were not consistent or statistically significant when compared across all eyes. Relative displacement differences were statistically significant between states, with corneal deturgescence and CXL favoring stiffer behavior and significant reductions in displacement variance. The mean values were 0.035 μm/μm in the edematous state, 0.021 μm/μm in the normal state, and 0.014 μm/μm in the CXL sate ($P<.05$, Tukey analysis). The Levene test indicated that the variance between the normal state and CXL state was statistically significantly different ($p<.05$). Figure 4 shows a box-and-stem plot of the resultant data.

DISCUSSION

In this serial-controlled human whole-globe study, we found that corneal edema and CXL both significantly affected the mechanical behavior of the cornea and that optical coherence elastography is capable of measuring these mechanical differences under physiologic stress conditions created by simple axial perturbations with a nonapplanating contact lens. In a study of lateral corneal displacement in human whole globes using surface mercury beads as fiducial markers, Hjortdal and Jensen[36] found very low lateral strains (~1.0%) indicative of high lateral stiffness under inflational stresses from 2 to 100 mm Hg. The low lateral-to-axial deformation ratios observed in the current study (1 to 3 μm of lateral displacement per 100 μm of axial displacement) confirm the very high relative stiffness of the normal cornea in the direction of the collagen lamellae, although with much lower imposed stresses and the added advantage of intrinsic pan-corneal optical fiducial features that allow displacement tracking across the entire corneal depth.

Abnormalities of corneal stromal resistance to deformation in the lateral direction have been proposed as a potential factor in the pathogenesis of corneal ectasia based on ultrastructural observations from x-ray diffraction,[37,38] second-harmonic-generation confocal microscopy,[39] and histology.[40] A recent x-ray diffraction study by Hayes et al.[41] suggests that ultrastructural changes, such as decreases in interfibrillar spacing and reduced fibril diameter observed after riboflavin–UVA CXL are dependent on the corneal hydration state and the relative osmolarity of the riboflavin solution. Porcine tissue studies have shown increases in corneal stiffness with dehydration[42,43] using excised cornea or corneal surface curvature changes under inflational stress. Recent studies using Brillouin microscopy,[44–47] which estimates elastic properties based on light-scattering behavior as opposed to displacement mapping, showed its capability to measure property changes after CXL in corneal tissue; however, no Brillouin-based data on the effects of hydration on corneal biomechanical properties have been reported. We believe that the present study is the first to nondestructively evaluate the dynamic impact of hydration and CXL treatment on the displacement behavior of the human corneal stroma in this direction of action.

Figure 4 shows that corneal deturgescence and CXL result in progressive and significant reductions in the mean lateral displacement and corresponding reductions in the spread of

the data. Although no statistically significant differences were observed regionally across all eye pairs, significant regional differences in relative displacement behavior were present in each eye. It is likely that the regional heterogeneity of and variation in these patterns from sample to sample in the deturgesed corneas is greater in postmortem human corneal tissue than in the in vivo state due to the lack of uniform endothelial cell function (as suggested by the regional variability in the upper elastogram in Figure 3, *A*), even with attempts to de-swell corneas to a physiologic CCT endpoint. It is also important to note that the measurement used to characterize local stiffness in these experiments is only 1 of many possible formulations of displacement behavior that can be derived from the measurements. The current measurement formulation was designed to be sensitive to differences in lateral strain, in the predominant direction of action of the collagen fibers. It is feasible that larger stresses with larger resulting displacements may facilitate better contrast for identifying local material property abnormalities for early keratoconus detection and other applications.

It is possible that depth-dependent variations like those observed in ex vivo tests of sectioned corneal tissue explants obtained from different stromal depths[3,48] were not consistently observed in this study because of the very low stresses applied. However, another important difference when comparing our results with those in previous studies is that the current approach measures the behavior of intact corneas surrounded by the native boundary conditions of the whole eye rather than of explants dissociated from their surrounding tissues. Winkler et al.[49] made the recent observation that the stromal collagen architecture may involve a greater degree of interconnectivity than previously recognized and that this interconnectivity may favor more homogenous tissue behaviors in intact in situ testing. We suspect the 4.0 mm scan diameter may also have contributed to the lack of significant regional differences across the groups because only a small portion of the total corneal stroma was measured. In future experiments, we plan to use a larger diameter lens and corresponding scan diameter to enable measurement of a large portion of the corneal stroma without being limited by the imaging aperture. We have also recently incorporated force sensors for more direct measurement of stress–strain relationships and local elastic modulus determination.

In summary, we report the first serial-control study of the effects of edema and CXL on stromal displacement behavior in human donor globes. These experiments showed significant increases in lateral corneal resistance with CXL and relative decreases in the presence of stromal edema. Optical coherence tomography–based elastography is sensitive enough to detect micron-level displacements with stresses comparable to those incurred during applanation tonometry and can be performed with a contoured contact surface to avoid complex bending moments, such as those produced during air puff–driven deformations. A reduction in corneal stromal resistance to lateral strain has been proposed as a potential mechanism of corneal instability in keratoconus, and the current study shows a potential biomechanical mechanism for increased corneal stability after CXL.

Acknowledgments

FINANCIAL DISCLOSURES

Mr. Ford and Drs. Rollins and Dupps are named on intellectual property relatedto the elastographymethod used inthis publication. Dr. Dupps is a consultant to Ziemer USA, Inc. and has received research funding from Avedro, Inc. and Carl Zeiss Meditec AG. Dr. Sinha Roy has no financial or proprietary interest in any material or method mentioned.

Supported in part by the National Institutes of Health (NIH) Visual Sciences Resource Center (CWRU) (P30 core grant EY11373) and the NIH Visual Sciences Training Program (grant T32 EY07157) (Case Western Reserve University); NIH (grant R01 EY023381 (Dr. Dupps); CTSA (grant UL1 RR024989) (Dr. Dupps); Research to Prevent Blindness Challenge and unrestricted grants to the Department of Ophthalmology, Cleveland Clinic Lerner College of Medicine; a Research to Prevent Blindness Career Development Award (Dr. Dupps), and an Ohio Third Frontier Innovation Platform Award to Cole Eye Institute, USA.

REFERENCES

1. Guirao A. Theoretical elastic response of the cornea to refractive surgery: risk factors for keratectasia. J Refract Surg. 2005; 21:176–185. [PubMed: 15796224]
2. Wollensak G, Spoerl E, Seiler T. Riboflavin/ultraviolet-A–induced collagen crosslinking for the treatment of keratoconus. Am J Ophthalmol. 2003; 135:620–627. Available at: http://grmc.ca/assets/files/collagen_crosslinking_2003_wollensak.pdf. [PubMed: 12719068]
3. Randleman JB, Dawson DG, Grossniklaus HE, McCarey BE, Edelhauser HF. Depth-dependent cohesive tensile strength in human donor corneas: implications for refractive surgery. J Refract Surg. 2008; 24:S85–S89. [PubMed: 18269156]
4. Luce DA. Determining in vivo biomechanical properties of the cornea with an ocular response analyzer. J Cataract Refract Surg. 2005; 31:156–162. [PubMed: 15721708]
5. Dupps WJ Jr, Netto MV, Herekar S, Krueger RR. Surface wave elastometry of the cornea in porcine and human donor eyes. J Refract. 2007; 23:66–75. Available at: http://www.ncbi.nlm.nih.gov/pmc/articles/PMC2075088/pdf/nihms-32896.pdf.
6. Andreassen TT, Simonsen AH, Oxlund H. Biomechanical properties of keratoconus and normal corneas. Exp Eye Res. 1980; 31:435–441. [PubMed: 7449878]
7. Roberts C. The cornea is not a piece of plastic [editorial]. J Refract Surg. 2000; 16:407–413. [PubMed: 10939720]
8. Dupps WJ Jr, Roberts C. Effect of acute biomechanical changes on corneal curvature after photokeratectomy. J Refract Surg. 2001; 17:658–669. [PubMed: 11758984]
9. Pallikaris IG, Kymionis GD, Astyrakakis NI. Corneal ectasia induced by laser in situ keratomileusis. J Cataract Refract Surg. 2001; 27:1796–1802. [PubMed: 11709254]
10. Dobbins KRB, Price FW Jr, Whitson WE. Trends in the indications for penetrating keratoplasty in the Midwestern United States. Cornea. 2000; 19:813–816. [PubMed: 11095055]
11. Ortiz D, Piñero D, Shabayek MH, Arnalich-Montiel F, Alió JL. Corneal biomechanical properties in normal, post-laser in situ keratomileusis, and keratoconic eyes. J Cataract Refract Surg. 2007; 33:1371–1375. [PubMed: 17662426]
12. Al-Towerki A-E, Gonnah E-S, Al-Rajhi A, Wagoner MD. Changing indications for corneal transplantation at the King Khaled Eye Specialist Hospital (1983–2002). Cornea 2004. 23:584–588.
13. Roy AS, Dupps WJ. Effects of altered corneal stiffness on native and postoperative LASIK corneal biomechanical behavior: a whole-eye finite element analysis. J Refract Surg. 2009; 25:875–887. [PubMed: 19835328]
14. Roy AS, Dupps WJ. Patient-specific modeling of corneal refractive surgery outcomes and inverse estimation of elastic property changes. J Biomech Eng. 2011; 133:011002. [PubMed: 21186892]
15. Dupps WJ Jr. Biomechanical modeling of corneal ectasia. J Refract Surg. 2005; 21:186–190. errata, 2007; 23:9. [PubMed: 15796225]
16. Ophir J, Céspedes I, Ponnekanti H, Yazdi Y, Li X. Elastography: a quantitative method for imaging the elasticity of biological tissues. Ultrason Imaging. 1991; 134:111–134. Available at: http://www.uth.tmc.edu/schools/med/rad/elasto/download/91/91Ophir.pdf. [PubMed: 1858217]
17. Adie SG, Kennedy BF, Armstrong JJ, Alexandrov SA, Sampson DD. Audio frequency in vivo optical coherence elastography. Phys Med Biol. 2009; 54:3129–3139. [PubMed: 19420415]

18. Adie SG, Liang X, Kennedy BF, John R, Sampson DD, Boppart SA. Spectroscopic optical coherence elastography. Opt Express. 2010; 18:25519–25534. Available at: http://www.opticsinfobase.org/oe/viewmedia.cfm?uriZoe-18-25-25519&seqZ0. [PubMed: 21164898]
19. De la Torre-Ibarra MHRuiz PD, Huntley JM. Double-shot depth-resolved displacement field measurement using phase-contrast spectral optical coherence tomography. Opt Express. 2006; 14:9643–9656. Available at: http://www.opticsinfobase.org/oe/viewmedia.cfm?uriZoe-14-21-9643&seqZ0. [PubMed: 19529355]
20. Kennedy BF, Liang X, Adie SG, Gerstmann DK, Quirk BC, Boppart SA, Sampson DD. In vivo three-dimensional optical coherence elastography. Opt Express. 2011; 19:6623–6634. Available at: http://www.ncbi.nlm.nih.gov/pmc/articles/PMC3308196/pdf/oe-19-7-6623.pdf. [PubMed: 21451690]
21. Kennedy BF, Hillman TR, McLaughlin RA, Quirk BC, Sampson DD. In vivo dynamic optical coherence elastography using a ring actuator. Opt Express. 2009; 17:21762–21772. Available at: http://www.opticsinfobase.org/oe/viewmedia.cfm?uriZoe-17-24-21762&seqZ0. [PubMed: 19997419]
22. Khalil AS, Chan RC, Chau AH, Bouma BE, Mofrad MRK. Tissue elasticity estimation with optical coherence elastography: toward mechanical characterization of in vivo soft tissue. Ann Biomed Eng. 2005; 33:1631–1639. [PubMed: 16341928]
23. Kirkpatrick SJ, Wang RK, Duncan DD. OCT-based elastography for large and small deformations. Opt Express. 2006; 14:11585–11597. Available at: http://www.opticsinfobase.org/oe/viewmedia.cfm?uriZoe-14-24-11585&seqZ0. [PubMed: 19529578]
24. Liang X, Orescanin M, Toohey KS, Insana MF, Boppart SA. Acoustomotive optical coherence elastography for measuring material mechanical properties. Opt Lett. 2009; 34:2894–2896. Available at: http://www.ncbi.nlm.nih.gov/pmc/articles/PMC2883315/pdf/nihms200389.pdf. [PubMed: 19794759]
25. Liang X, Oldenburg A, Crecea V, Chaney E. Optical micro-scale mapping of dynamic biomechanical tissue properties. Opt Express. 2008; 16:11052–11065. Available at: http://www.opticsinfobase.org/oe/viewmedia.cfm?uriZoe-16-15-11052&seqZ0. [PubMed: 18648419]
26. Liang X, Boppart SA. Biomechanical properties of in vivo human skin from dynamic optical coherence elastography. IEEE Trans Biomed Eng. 2010; 57:953–959. Available at: http://www.ncbi.nlm.nih.gov/pmc/articles/PMC3699319/pdf/nihms467017.pdf. [PubMed: 19822464]
27. Oldenburg AL, Toublan FJ-J, Suslick KS, Wei A, Boppart SA. Magnetomotive contrast for in vivo optical coherence tomography. Opt Express. 2005; 13:6597–6614. Available at: http://biophotonics.illinois.edu/pubs/biophotonics_current/magnetomotivecontrast.pdf. [PubMed: 19498675]
28. Rogowska J, Patel NA, Fujimoto JG, Brezinski ME. Optical coherence tomographic elastography technique for measuring deformation and strain of atherosclerotic tissues. Heart. 2004; 90:556–562. Available at: http://www.ncbi.nlm.nih.gov/pmc/articles/PMC1768234/pdf/hrt09000556.pdf. [PubMed: 15084558]
29. Rogowska J, Patel N, Plummer S, Brezinski ME. Quantitative optical coherence tomographic elastography: method for assessing arterial mechanical properties. Br J Radiol. 2006; 79:707–711. [PubMed: 16793852]
30. Schmitt JM. OCT elastography: imaging microscopic deformation and strain of tissue. Opt Express. 1998; 3:199–211. Available at: http://www.opticsinfobase.org/oe/viewmedia.cfm?uriZoe-3-6-199&seqZ0. [PubMed: 19384362]
31. Van Soest G, Mastik F, de Jong N, van der Steen AFW. Robust intravascular optical coherence elastography by line correlations. Phys Med Biol. 2007; 52:2445–2458. [PubMed: 17440245]
32. Ford MR, Dupps WJ Jr, Rollins AM, Sinha Roy A, Hu Z. Method for optical coherence elastography of the cornea. J Biomed Opt. 2011; 16:016005. Available at: http://www.ncbi.nlm.nih.gov/pmc/articles/PMC3041813/pdf/JBOPFO-000016-016005_1.pdf. [PubMed: 21280911]
33. Armstrong BK, Lin MP, Ford MR, Santhiago MR, Singh V, Grossman GH, Agrawal V, Sinha Roy A, Butler RS, Dupps WJ, Wilson SE. Biological and biomechanical responses to traditional epithelium-off and transepithelial riboflavin-UVA CXL techniques in rabbits. J Refract Surg. 2013; 29:332–341. [PubMed: 23659231]

34. Duffey RJ, Tchah H, Lindstrom RL. Human cadaver corneal thinning for experimental refractive surgery. Refract Corneal Surg. 1989; 5:41–42. [PubMed: 2484949]
35. Terry MA, Ousley PJ, Zjhra ML. Hydration changes in cadaver eyes prepared for practice and experimental surgery. Arch Ophthalmol. 1994; 112:538–543. [PubMed: 7512337]
36. Hjortdal JØ, Jensen PK. In vitro measurement of corneal strain, thickness, and curvature using digital image processing. Acta Ophthalmol Scand. 1995; 73:5–11. [PubMed: 7627759]
37. Meek KM, Tuft SJ, Huang Y, Gill PS, Hayes S, Newton RH, Bron AJ. Changes in collagen orientation and distribution in keratoconus corneas. Invest Ophthalmol Vis Sci. 2005; 46:1948–1956. Available at: http://www.iovs.org/content/46/6/1948.full.pdf. [PubMed: 15914608]
38. Akhtar S, Bron AJ, Salvi SM, Hawksworth NR, Tuft SJ, Meek KM. Ultrastructural analysis of collagen fibrils and proteoglycans in keratoconus. Acta Ophthalmol. 2008; 86:764–772. Available at: http://onlinelibrary.wiley.com/doi/10.1111/j.1755-3768.2007.01142.x/pdf. [PubMed: 18422999]
39. Morishige N, Wahlert AJ, Kenney MC, Brown DJ, Kawamoto K, Chikama T-i, Nishida T, Jester JV. Second-harmonic imaging microscopy of normal human and keratoconus cornea. Invest Ophthalmol Vis Sci. 2007; 48:1087–1094. Available at: http://www.iovs.org/content/48/3/1087.full.pdf. [PubMed: 17325150]
40. Dawson DG, Randleman JB, Grossniklaus HE, O'Brien TP, Dubovy SR, Schmack I, Stulting RD, Edelhauser HF. Corneal ectasia after excimer laser keratorefractive surgery: histopathology, ultrastructure, and pathophysiology. Ophthalmology. 2008; 115:2181–2191. [PubMed: 18692245]
41. Hayes S, Boote C, Kamma-Lorger CS, Rajan MS, Harris J, Dooley E, Hawksworth N, Hiller J, Terill NJ, Hafezi F, Brama AK, Wuantock AJ, Meek KM. Riboflavin/UVA collagen cross-linking-induced changes in normal and keratoconus corneal stroma. PLoS One. 2011; 6:e22405. Available at: http://www.plosone.org/article/fetchObject.action?uriZinfo%3Adoi%2F10.1371%2Fjournal.pone.0022405&representation=PDF. [PubMed: 21850225]
42. Hatami-Marbini H, Etebu E. Hydration dependent biomechanical properties of the corneal stroma. Exp Eye Res. 2013; 116:47–54. [PubMed: 23891861]
43. Kling S, Marcos S. Effect of hydration state and storage media on corneal biomechanical response from in vitro inflation tests. J Refract Surg. 2013; 29:490–497. [PubMed: 23820232]
44. Scarcelli G, Yun SH. In vivo Brillouin optical microscopy of the human eye. Opt Express. 2012; 20:9197–9202. Available at: http://www.opticsinfobase.org/oe/viewmedia.cfm?uriZoe-20-8-9197&seqZ0. [PubMed: 22513631]
45. Scarcelli G, Pineda R, Yun SH. Brillouin optical microscopy for corneal biomechanics. Invest Ophthalmol Vis Sci. 2012; 53:185–190. Available at: http://www.iovs.org/content/53/1/185.full.pdf. [PubMed: 22159012]
46. Scarcelli G, Kling S, Quijano E, Pineda R, Marcos S, Yun SH. Brillouin microscopy of collagen crosslinking: noncontact depth-dependent analysis of corneal elastic modulus. Invest Ophthalmol Vis Sci. 2013; 54:1418–1425. Available at: http://www.iovs.org/content/54/2/1418.full.pdf. [PubMed: 23361513]
47. Kling S, Remon L, Pérez-Escudero A, Merayo-Lloves J, Marcos S. Corneal biomechanical changes after collagen cross-linking from porcine eye inflation experiments. Invest Ophthalmol Vis Sci. 2010; 51:3961–3968. Available at: http://www.iovs.org/content/51/8/3961.full.pdf. [PubMed: 20335615]
48. Winkler M, Chai D, Kriling S, Nien CJ, Brown DJ, Jester B, Juhasz T, Jester JV. Nonlinear optical macroscopic assessment of 3-D corneal collagen organization and axial biomechanics. Invest Ophthalmol Vis Sci. 2011; 52:8818–8827. Available at: http://www.iovs.org/content/52/12/8818.full.pdf. [PubMed: 22003117]
49. Winkler M, Shoa G, Xie Y, Petsche SJ, Pinsky PM, Juhasz T, Brown DJ, Jester JV. Three-dimensional distribution of trans-verse collagen fibers in the anterior human corneal stroma. Invest Ophthalmol Vis Sci. 2013; 54:7293–7301. [PubMed: 24114547]

WHAT WAS KNOWN

- Commercially available clinical devices for estimating corneal biomechanical properties do not monitor deformation of intracorneal deformations.
- This limits the ability to obtain depth-dependent stromal biomechanical property data and does not facilitate the resolution of lateral displacement, which may be important in ectasia screening and detection of CXL-mediated effects.
- Previous studies report differences in the elastic behavior of nonhuman corneal specimens with altered corneal hydration.

WHAT THIS PAPER ADDS

- Optical coherence tomography–based elastography was sensitive enough to detect micron-level displacements without the need for destructive or nonphysiologic stressors that invoke large displacements.
- The results confirm the high stiffness of the cornea in the direction of the collagen lamellae while demonstrating for the first time in human tissue that significant changes in lateral resistance occur with edema and after CXL. Increases in lateral stiffness may be an important mechanism of corneal topographic stability after CXL.

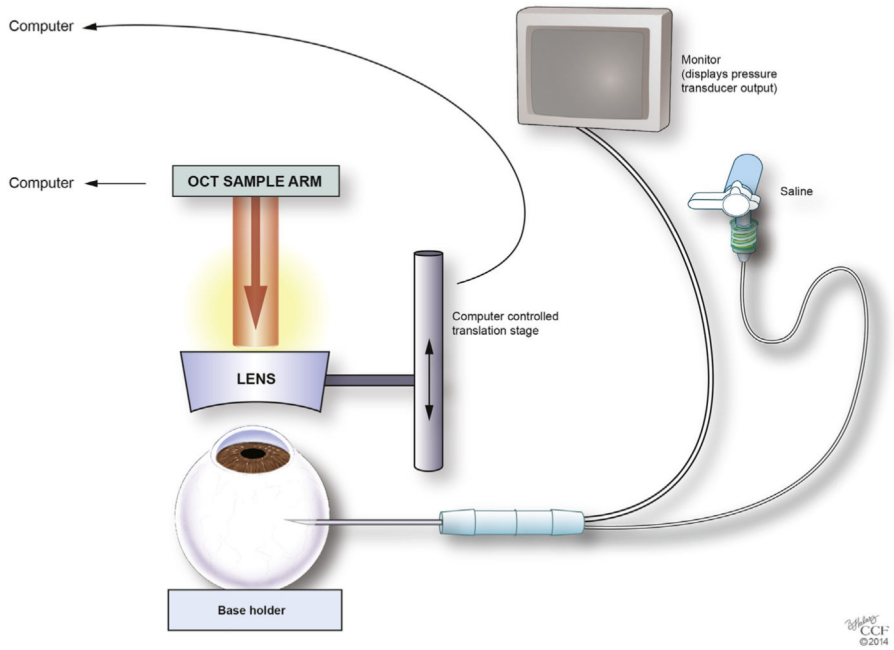

Figure 1.

Three-dimensional representation of the gonioscopy lens and whole globe in the OCT sample arm path with mechanically translating mobile arm attached.

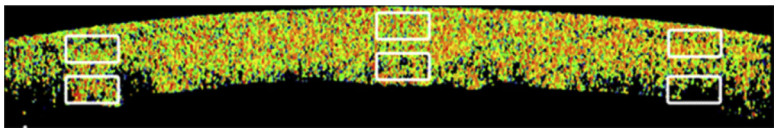

Figure 2.
Color elastogram of the approximate regions of interest defined for statistical comparisons.

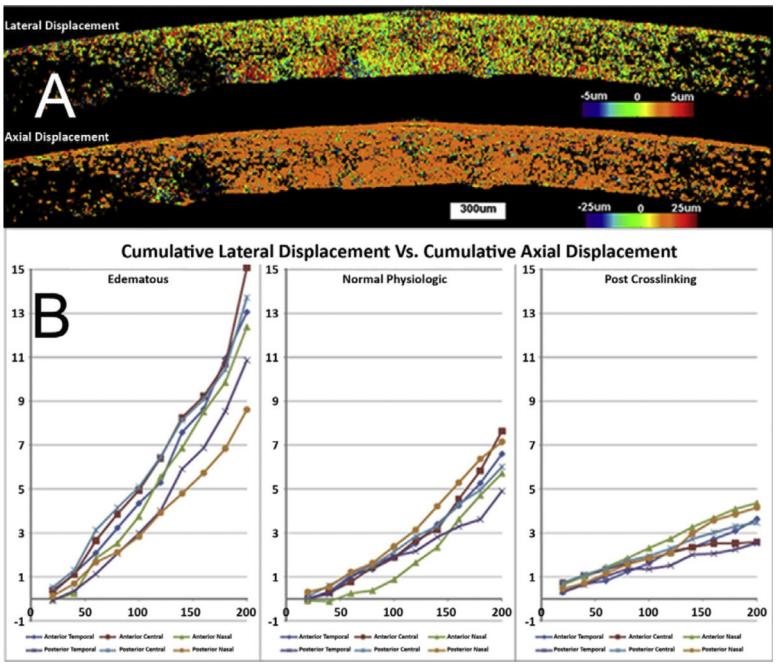

Figure 3.

A: Examples of axial and lateral displacement maps for a single eye in the post-deturgescence state. Lateral displacements (*top frame*) and axial displacements (*bottom frame*) are presented (in μm) for a 20 μm axial compression. The axial displacement data show a measured group displacement of approximately 20 μm. *B*: Cumulative regional corneal displacements for the nasal–temporal meridian of the same eye in *A*. Lateral to axial displacement ratios for the edematous state, deturgesed state, and post-CXL state are plotted for serial compressions. Each line corresponds to one of the 6 defined regions of interest within the same 2-dimensional section of the cornea.

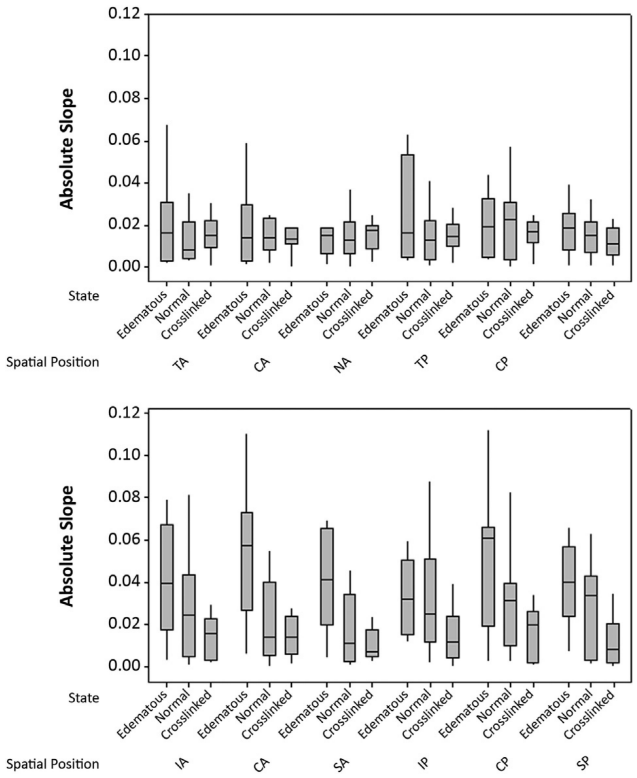

Figure 4.

Distribution of the absolute displacement slope in all eyes in all states. In this standard box-and-whisker plot, the central line indicates the median of the data, the box represents the 2nd and 3rd quartiles, and the whiskers indicate the 1st and 4th quartiles. Lower slope values indicate a relative reduction in lateral displacement for a given imposed axial perturbation. *Top*: Nasal to temporal orientation. *Bottom*: Superior to inferior orientation (CA = central anterior; CP = central posterior; IA = inferior anterior; IP = inferior posterior; NA = nasal anterior; NP = nasal posterior; SA = superior anterior; SP = superior posterior; TA = temporal anterior; TP = temporal posterior).

Table 1

Mean absolute slope of displacements (measured lateral tissue displacement/imposed axial displacement perturbation) for each region of the cornea in all 3 measured states from the final 4 eye pairs.

	Mean (μm/μm) ± SD		
Spatial Position	**Edematous Cornea**	**Normal Cornea**	**Crosslinked Cornea**
Anterior nasal	0.039 ± 0.052	0.019 ± 0.020	0.015 ± 0.009
Anterior central	0.038 ± 0.031	0.023 ± 0.025	0.015 ± 0.01
Anterior temporal	0.035 ± 0.043	0.017 ± 0.014	0.013 ± 0.007
Posterior nasal	0.034 ± 0.034	0.024 ± 0.023	0.015 ± 0.001
Posterior central	0.035 ± 0.030	0.024 ± 0.019	0.016 ± 0.01
Posterior temporal	0.032 ± 0.031	0.021 ± 0.016	0.012 ± 0.009